A Multiwavelength Investigation of the Relationship Between 2CG 135+1 and LSI+61° 303

M. S. Strickman[1], M. Tavani[2], M. J. Coe[3], I. A. Steele[4], J. Fabregat[5], J. Martí[6], J. M. Paredes[7], P. S. Ray[1,8]

ABSTRACT

We present the results of a multiwavelength monitoring campaign targeting the γ-ray source 2CG 135+1 in an attempt to confirm the association of this object with the radio/Be/X-ray binary system LSI +61°303. The campaign included simultaneous radio, optical, infrared, and hard x-ray/γ-ray observations carried out with a variety of instruments, covering (not continously) almost three binary cycles of LSI +61°303 during the period April-July 1994. Three separate OSSE observations of the γ-ray source were carried out, covering different phases of the radio lightcurve. Hard X-ray/γ-ray emission was detected from the direction of 2CG 135+1 during the first of these OSSE observations. The signal to noise ratio of the OSSE observations was insufficient to establish a spectral or intensity correlation of the high-energy emission with simultaneous radio, optical and infrared emission of LSI +61°303. We briefly discuss the theoretical implications of our observations.

Subject headings: X-rays: binaries

[1]Naval Research Laboratory, Washington, DC 20375-5352; strickman@osse.nrl.navy.mil

[2]Columbia Astrophysics Laboratory, Columbia University, New York, NY 10027; tavani@astro.columbia.edu

[3]Department of Physics and Astronomy, University of Southampton, Southampton, SO17 1BJ, U.K.; mjc@astro.soton.ac.uk

[4]Astrophysics Group, Liverpool John Moores University, Liverpool, L3 3AF, U.K.; ias@staru1.livjm.ac.uk

[5]Departmento de Astronomia, Universidad de Valencia, 46100 Burjassot, Spain; fabregat@evalvx.ific.uv.es

[6]CEA/DSM/DAPNIA/Service d'Astrophysique, Centre d'Études de Saclay,91191 Gif-Sur-Yvette CEDEX,FRANCE

[7]Departament d'Astronomia i Meteorologia, Universitat de Barcelona, Av. Diagonal 647, E-08028, Barcelona, Spain; josepmp@mizar.am.ub.es

[8]NRC Research Associate; paulr@rira.nrl.navy.mil

1. Introduction

The γ-ray source 2CG 135+1 is one of the most prominent unidentified γ-ray sources near the Galactic plane. Since its discovery by the COS-B satellite (Hermsen et al. 1977, Swanenburg et al. 1981), no satisfactory explanation has been found for the nature of 2CG 135+1 and its γ-ray emission mechanism. The COS-B error box of 2CG 135+1 contains two interesting sources, the radio flaring Be star LSI +61°303, and the QSO 0241+622 (e.g, Perotti et al. 1980). EGRET observations of 2CG 135+1 during CGRO Phase 1 and 2 (von Montigny et al. 1993, Thompson et al. 1995, Kniffen et al. 1997) resulted in a $\sim 20'$ wide error box location. The source appeared in the 2nd EGRET catalog as 2EG J0241+6119 (Thompson et al. 1995). The new EGRET position of the γ-ray source is well within the COS-B error box and is consistent with the position of LSI +61°303. The position of the QSO 0241+622 is outside the newly established γ-ray error box, being about $50'$ away from the centroid of the EGRET error box (Kniffen et al. 1997). COMPTEL Phase 1 and 2 observations also confirmed the presence of a γ-ray source consistent with the position of 2EG J0241+6119 in the energy range 1–30 MeV (van Dijk et al. 1996). Due to their limited angular resolution, COMPTEL observations cannot rule out either LSI +61°303 or QSO 0241+622 as a possible counterpart of the γ-ray source.

The remarkable system LSI +61°303 (GT 0236 +610, V615 Cas) is one of the few Be/X-ray binary stars which exhibits strong radio emission. The periodic nature of this radio emission was first determined by Taylor & Gregory (1982) who found it to be strongly modulated with a period of $\sim$ 26.5 days. The currently accepted value of the radio period is 26.496 ± 0.008 days (Taylor & Gregory 1984). Radio phase zero has been arbitrarily set at Julian Date 2443366.775 for the system with the radio outbursts occuring normally at phases 0.5 – 0.7. Spectroscopic radial velocities (Hutchings & Crampton 1981) for the system indicate that the $\sim$ 26.5 day modulation corresponds to the orbital period of the binary system. Modulation of the IR and optical system at the radio period has been reported by Paredes et al. (1994).

Optical spectra of the source are typical of a Be system, showing strong emission in the Hα and Hβ lines. Also typical of a Be star is the infrared excess observed from the system (Martí & Paredes 1995). Both of these observations are generally explained in Be systems by some form of equatorially enhanced stellar wind (i.e. circumstellar disk) surrounding the Be star. This circumstellar disk is thought to be the source of the material accreting onto the neutron star in Be/X-ray binaries.

Soft X-ray emission in the range 0.5-5 keV from LSI +61°303 was detected by *Einstein* (Share et al. 1979, Bignami et al. 1981), and recent ASCA (Leahy, Harrison & Yoshida 1996; Harrison, Leahy & Waltman 1996) and ROSAT (Goldoni & Mereghetti 1995, Taylor et al. 1996) observations confirm the detection. Recent analysis of public ASM/RXTE data (Paredes et al. 1997) has shown that the X-ray emission also appears to display outbursts with the same period as the radio. These data show clear evidence for a 26.7 ± 0.2 d period, the folded X-ray light curve exhibiting a broad high state overlapping the usually active radio phases.

Assuming 2CG 135+1 is associated with LSI +61°303 rather than the QSO, various possible models of the γ-ray production mechanism have been proposed. Recent models include a non-accreting young pulsar in a system with a mass-losing B-star (Maraschi & Treves (1981), Tavani (1995, 1997)), and super-Eddington accretion onto a neutron star (Martí & Paredes 1995).

In an attempt to confirm the association between the γ-ray source and LSI +61°303 and to provide input data for modeling of the system, simultaneous γ-ray, radio, optical, and infrared observations were obtained during the interval 1994 April–July. The OSSE instrument on the *Compton Gamma-Ray Observatory* (CGRO) performed a series of hard X-ray/γ-ray pointings centered at 2CG 135+1 during April and again during June and July, 1994. Frequent radio observations of LSI +61°303 were carried out at the Green Bank Interferometer (GBI) and during June and July at the VLA. Likewise, optical spectroscopy was obtained from the Jacobus Kapteyn Telescope (JKT), La Palma and infrared photometry from the Carlos Sánchez Telescope (TCS), Tenerife during late June and early July, 1994. This paper presents the results of all of these observations and discusses their implications for the various proposed models of the system.

2. Observations

2.1. OSSE Observations

OSSE observed the region containing LSI +61°303 on three occasions from 1994 April to July, as shown

in Table 1. OSSE, described by Johnson et al. (1993) consists of four nearly identical NaI detectors, of which two were in use for these observations. The OSSE field-of-view (FOV) is $3.^\circ8 \times 11.^\circ4$, large enough that source confusion is a concern, especially near the galactic plane. Figure 1 shows the OSSE viewing configuration for the three observations. Note that we cannot unambiguously determine whether any detected emission belongs to LSI +61°303 or to QSO 0241+622 from positional considerations alone.

In Figure 2 we present the derived OSSE light curves for the three viewing periods, together with radio light curves from the GBI. Figure 3 displays the OSSE spectrum from VP 325. OSSE detected a signal with $\simeq 4\sigma$ significance from the direction of LSI +61°303 in the 50–300 keV band during VP 325. No significant signal was detected from this region during VP 330 or VP 332. The resulting upper limits, listed in Table 2, are consistent with the VP 325 detection, hence the OSSE data do not strongly support a claim of time variability from one viewing period to the next, nor is there any obvious correlation between the hard X-ray and radio light curves. However, we also note that the OSSE data for VP 325 are inconsistent with a constant flux at the 99% confidence level.

The OSSE spectrum, shown in Figure 3, is well represented by a power-law model with photon index 1.6±0.6 over the 50–300 keV range. In order to estimate the contribution of the diffuse galactic continuum emission to the observed signal, we have used a model normalized to OSSE galactic plane observations (Skibo 1996, private communication). The resulting estimated contribution, at least an order of magnitude less than the observed flux, is negligible. In addition, contributions from the binary X-ray pulsar 4U 0115+63, which was located on the edge of one of the background fields during VP 325 (see Figure 1), are negligible. A major outburst from this source took place just after the end of VP 325 (Negueruela, et al. 1997). Although the source was still active during VP 330 and VP 332, the viewing configuration for these periods excluded 4U0115+63 as a potential contaminant.

2.2. Radio Observations

2.2.1. Green Bank Interferometer

The Green Bank Interferometer (GBI) began a program of continuous daily monitoring of LSI +61°303 in 1994 January which continued until 1996 February. For a complete description of these observations see Ray et al. (1997). Briefly, the GBI consists of two 26 m antennas on a 2.4 km baseline, each of which has a pair of cooled 35 MHz bandwidth receivers to simultaneously receive signals at 2.25 and 8.3 GHz. Ten minute observations of LSI +61°303 were performed 1–10 times per day within ±5 hours of source transit. Measured correlator amplitudes are converted to flux densities by comparison to standard, regularly observed calibrators. Flux densities from the GBI monitoring are available during all of the OSSE viewing periods. Figure 2 shows daily averages of the GBI data.

2.2.2. VLA Observations

In addition to the Green Bank Data, the VLA interferometer was used to monitor the radio emission of LSI +61°303 throughout a full orbital period of 26.5 d concurrent with the OSSE observations in VP 332. Sixteen VLA observing sessions were carried out, evenly spaced by a few days, and covering the time interval from 1994 June 9 to 1994 July 8. Each session had a typical duration between 2–4 h and allowed us to measure the LSI +61°303 flux density at up to 5 different radio wavelengths (20, 6, 3.5, 2.0 and 1.3 cm). The VLA was always in the B configuration. During the two shortest sessions available only three wavelengths were observed (20, 6 and 3.5 cm), while in some cases it was possible to include a few additional 90 cm measurements. For all observations, a bandwidth of 100 MHz was employed except at 90 cm, where a smaller bandwidth of 6 MHz was selected. The data were edited and calibrated using the AIPS software package. The source 3C48 was always used as absolute amplitude calibrator, while the phase calibrator adopted at all wavelengths was 0228+673, except at 90 cm where 0229+777 was used instead. In most observations LSI +61°303 appeared as an isolated strong point source, allowing us to use phase self calibration to improve the dynamic range of the maps from which flux densities were measured.

The results of the VLA radio monitoring are given in Table 3. The flux density errors quoted in columns three through eight are the rms noise of the map in mJy beam^{-1}. The data listed in Table 3 are also plotted in the panels of Figure 4 in the form of radio light curves for the different wavelengths, showing the development of the radio outburst. The time evolution of the radio spectrum is displayed in the panels of Figure 5 for each observing session. A power law

model spectrum has been fit to each spectrum. Significant phase-dependent deviations from the power law, especially at the lowest and highest frequencies, are evident in this figure. In order to discuss these effects in more detail, we have plotted spectral indices between adjacent wavelength pairs, in addition to the best fit power law index, as a function of radio phase (Figure 6).

2.3. Optical Spectroscopy

Optical spectra of LSI +61°303 in the regions of the Hα, Hβ and Hγ lines were obtained during the period 1994 June 25 – 28. The observations were made using the Richardson-Brearly Spectrograph (Edwin 1988) of the Jacobus Kapteyn Telescope, La Palma with the EEV7 CCD detector. The dispersion was 0.8Å per pixel, and, from observations of narrow interstellar features in our spectra, we estimate the spectral resolution was less than 2Å in all our observations. A log of the observations is given in Table 6. Data reduction was carried out according to standard spectroscopic procedures using the STARLINK supported package FIGARO (Shortridge 1991). The spectra were flux calibrated with observations of standards from Oke & Gunn (1983). No attempt was made to remove atmospheric absorption features from the spectra because these lines do not contaminate the regions of interest for this work. In Figures 7 and 8, we plot excerpts from the spectra showing the Hα, β and γ lines. We discuss model fitting to these spectra in a later section.

2.4. Infrared Photometry

Infrared J ($\sim$ 1.2μm), H ($\sim$ 1.6μm) and K ($\sim$ 2.2μm) observations of LSI +61°303 were obtained from the Carlos Sánchez Telescope (TCS), Tenerife during the period 1994 June 21 – 1994 July 1 using the CVF infrared photometer. The observations are listed in Table 5 and plotted in Figure 9. Observations on the last night are of poorer quality due to dust in the atmosphere. A clear trend in the data is apparent, with the infrared flux brightening during the period from radio phase $\sim$ 0.4–0.6. At later phases, our data are consistent with either constant or declining infrared flux.

3. Discussion

3.1. The OSSE Results

To place the OSSE observation in the context of other observations at different energies, Figure 3 includes noncontemporaneous results from COMPTEL (Van Dijk et al. 1996), EGRET (Thompson et al. 1995), and ASCA (Leahy et al. 1996). (Note that COMPTEL cannot resolve LSI +61°303 from QSO 0241+622). Although we have not displayed the MISO result (Perotti et al. 1980), it clearly exhibits a higher flux than either the OSSE or COMPTEL observations. However, due to the low detection significance of all these data, it is difficult to conclude that the MISO result is inconsistent at more than a 3σ confidence level. We have extrapolated the ASCA 1–10 keV best fit power law models from two observations (radio phase 0.2 and 0.42) into the OSSE energy range. Observations by Goldoni & Mereghetti (1995) using the ROSAT PSPC cover too low an energy range to usefully extrapolate to γ-rays, especially considering possible correlation of column density and power law index in their best fit result. The ASCA result, on the other hand, extends well above the energy band where absorption is effective, and therefore supplies a better measure of the underlying power law. As suggested by Leahy et al. (1996), the extrapolation predicts considerably less emission in the OSSE range than was observed. The OSSE integral flux from 50–300 keV during VP 325 is $(4.3\pm1.1)\times10^{-4}$ photons cm^{-2} s^{-1}, while the integral of the ASCA best fit power law models extrapolated to the same energy range are $(1.0 \pm 0.4) \times 10^{-4}$ and $(0.5 \pm 0.2) \times 10^{-4}$ photons cm^{-2} s^{-1} for radio phases 0.2 and 0.42 respectively. These are inconsistent at the 2.8σ and 3.4σ levels, assuming that the spectrum does not change (in particular, does not harden significantly) from 10 keV to 300 keV.

Since the relatively large OSSE field-of-view does not exclude the nearby QSO 0241+622 as a possible source of emission, we have also plotted the result of EXOSAT (2 – 10 keV) observations of the QSO (Turner & Pounds 1989), corrected for the its position in the OSSE collimator response. Note that the 1.7 photon index power law spectrum used to model the EXOSAT data is consistent with the the OSSE result.

When we look at an overall view of the spectra from this region, no clear picture emerges. However, the fact that OSSE and COMPTEL results fall significantly above an extrapolation of the ASCA spectra

and that the OSSE and COMPTEL spectra are consistent with the X-ray spectrum of QSO 0241+622, lead to the likelihood that at least some, and perhaps a significant amount, of the flux observed by both OSSE and COMPTEL might come from the QSO rather than LSI +61°303. Cycle-to-cycle variations in the X-ray emission may also contribute to the observed discrepancy. More contemporaneous X-ray and γ-ray data are required to test for the existence of cycle to cycle variability of the LSI +61°303 system and to better study the X-ray period recently reported by Paredes et al. (1997).

Similarly, the low significance of the OSSE light curves shown in Figure 2 does not allow us to use temporal signatures to associate LSI +61°303 with the OSSE source. We note that the flux detected by OSSE is relatively higher during the April 1994 observation, in apparent coincidence with a prominent onset and slow decay of a radio flare. June 1994 observations show a null detection in the BATSE energy range in coincidence with an extended minimum of the radio light curve. July 1994 observations by OSSE show a fluctuating low-intensity γ-ray flux in coincidence with the onset and decay of another radio flare. We see little of no evidence of γ-ray emission before the radio flare during July, although the X-ray evidence (e.g. Paredes et al. 1997, Leahy et al. 1996) indicates that the high energy flare preceeds the radio. We are therefore unable to use either spectral or temporal OSSE information to unambiguosly associate the γ-ray emission from this region of the sky with LSI +61°303.

3.2. Model Constraints

Assuming 2CG 135+1 is associated with the radio/X-ray source, we may ask if our observations place any constraints on two proposed models of the system currently under debate.

In the first model LSI +61°303 is assumed to contain a non-accreting young pulsar in orbit around the mass-losing Be-star (e.g. Maraschi & Treves 1981, Tavani 1995). In this case the high energy emission results from the interaction of the pulsar wind with the circumstellar material surrounding the Be star, a mechanism which has recently been shown to operate in the Be star/pulsar system PSR 1259-63 (Tavani & Arons 1997). The modulation of the radio emission may be due to the the time-variable geometry of a 'pulsar cavity' as a function of orbital phase. Ultimately the high-energy shock emissivity will depend on the geometrical and radiative characteristics of the pulsar cavity as the pulsar orbits around the primary. Long timescale modulations in the emission from the system are explained by the influence of a time variable mass outflow from the Be star, and its effect on the size of the pulsar cavity and its emissions.

The second model for the LSI +61°303 system proposes that the high energy emission results from super-Eddington accretion of the circumstellar material surrounding the Be star onto a neutron star (e.g. Taylor et al. 1992, Martí & Paredes 1995). As well as producing the high energy photons, this is assumed to result in a stream of relativistic particles which cool by synchrotron emission, resulting in the radio emission. The modulation of the radio light curve is assumed to be due to the relativistic electrons only being accelerated during a short period (or periods) of each orbit, with wind optical depth effects dictating the time delay between the injection of the electrons and the visibility of the radio emission.

We shall now consider (at least qualitatively) whether each of the proposed models can explain the observed features of the phase resolved radio and X-ray spectra.

3.2.1. Non-accreting pulsar model

The pulsar model for 2CG 135+1 is based on a *non-accreting* high-energy source. A rapidly rotating pulsar, as expected in young binary systems located near the Galactic plane, can be sufficiently energetic to avoid accretion of gaseous material provided by the mass outflow of a massive companion star. A relativistic pulsar wind, made of electron/positrons (possibly ions) and electromagnetic fields can sweep away the gaseous material from the Be star companion and produce high-energy emission by a relativistic shock. This mechanism of high-energy emission is believed to power the unpulsed X-ray and γ-ray emission from the Crab nebula (Nolan et al., 1993), and it was recently demonstrated to fit the time variable high-energy emission observed near periastron from the Be star/pulsar system PSR B1259-63 (Tavani & Arons 1997, hereafter TA97). PSR B1259-63, a 47 ms pulsar of moderately high spindown power in a long-period (3.4 yrs), high eccentricity ($\sim$ 0.87) orbit around a Be star, is particularly suited for our discussion. Time variable soft and hard X-ray energy emission has been detected throughout the PSR B1259-63 orbit, with luminosities in the range $10^{33} - 10^{34}\,\mathrm{erg\,s^{-1}}$ (TA97 and references therein). All the character-

istics of the high-energy emission from this system are in agreement with the expectations from a shock-driven emission mechanism. In particular, the lack of strong X-ray emission, lack of Fe line emission, and the small and constant column density of the PSR B1259-63 system throughout its elliptical orbit ($N_H \sim 6 \cdot 10^{21}\,\mathrm{cm}^{-2}$, comparable to LSI +61°303, see Leahy et al., 1996) strongly argue against an accretion-driven interpretation of the observations. In the case of the PSR B1259-63 system, the pulsar and binary characteristics conspire to produce a synchrotron power-law emission up to ~ 1 MeV and negligible inverse Compton scattering in the EGRET energy range, in agreement with observations (TA97). However, the features of the high-energy emission of the PSR B1259-63 system are not unique, and emission in the COMPTEL-EGRET energy range is expected from a more energetic pulsar orbiting around a Be star (Tavani 1995, 1997). 2CG 135+1 may be such a system. In analogy with the case of the PSR B1259-63 system, the low-energy emission below ~ 1 MeV can be powered by synchrotron emission from a shock at intermediate distance between the pulsar and the Be star surface. Emission in the EGRET energy range can be produced by inverse Compton scattering of soft photons (both from the synchrotron component at the shock and from the Be star surface and/or equatorial disk) against the relativistic particle flow. Modulation of the high-energy flux from 2CG 135+1 is expected in this model, depending on the geometry of the pulsar cavity (Maraschi & Treves 1981) and/or pitch angle anisotropy distribution of relativistic particles advected away from the shock site (TA97). An overall time variability of the high-energy flux is also expected as a function of a variable mass outflow rate from the Be star companion (Tavani 1995, 1997). In this model, radio emission can result from the relativistic particles of the pulsar wind advected away from the 'nose' of the pulsar cavity. This radio emission (a combination of synchrotron and inverse Compton emission from moderately relativistic electrons/positrons in the pulsar wind) is expected to be enhanced at selected orbital phases depending on the geometry. Substantial radio enhancement and 'flaring' can occur in coincidence with orbital phases corresponding to the line of sight being almost aligned with the axis of the 'comet-like' pulsar cavity in the Be star outflow. Many of the considerations of the next section on synchrotron and inverse Compton losses of radio emitting particles can be applied also in this context.

Our OSSE observations constrain the synchrotron contribution to the emission from 2CG 135+1 to be marginally consistent and not larger than what observed in the 50-200 keV range in the case of the periastron passage of PSR B1259-63. The hard X-ray emission from 2CG 135+1 in coincidence with the onset and decay of the radio flares of LSI +61°303 (not necessarily corresponding to the periastron) is therefore constrained to be below $10^{34}\,\mathrm{erg\,s}^{-1}$. We notice here that a featureless power-law spectrum in the X-ray range is what is expected by a relativistic shock model of emission in a pulsar binary (TA97).

3.2.2. Super-Eddington model

To test the super-Eddington accretion/particle-injection model we assume the radio emission can be attributed to synchrotron radiation from relativistic electrons in hot ionized clouds (plasmons), with the electrons accelerated either by shocks in gas dynamical expansions or by the magnetosphere of the compact companion (Penninx 1989). The radio light curves of LSI +61°303 shown in Figures 2 and 4 have a shape dominated by the occurrence of the expected periodic radio outburst, between radio phases 0.4 and 1.0. This main flaring event was preceded by at least two minor outbursts, at phases 0.1 and 0.3. In addition, the 1.3 cm data suggests that there was a third minor outburst, centered around phase 0.8, whose radio emission overlaps with the decay of the main event. The expected radio spectrum is a non-thermal power law with a negative spectral index α ($S_\nu \propto \nu^\alpha$). In general terms, the spectral indices shown in Figure 6 do agree with this expectation. However, deviations from simple power law behavior are evident in our data (see Figure 5), and they seem to be clearly related with the state of radio activity of the source. In this way, during the observed periods of low radio activity (phases 0.0-0.3 and 0.9-0.1), the radio spectrum between 20, 6 and 3.5 cm is well represented as a simple power law of spectral index $\alpha \simeq -0.5$. However, during the flaring interval (phases 0.3-0.9), the spectral indices undergo noticeable variations especially at both ends of the spectrum.

The changes of $\alpha_{20-6\mathrm{cm}}$ are probably due to opacity effects, i.e., the development of an optically thick synchrotron spectrum during the rise of the main outburst. This kind of behavior has been previously observed in other outbursts of this source (Taylor & Gregory, 1984; Taylor et al., 1995) and may be at-

tributed to synchrotron self-absorption in the radio emitting plasmon during the early stages of the outburst. The plots of spectral index in Figure 2 and $\alpha_{20-6\mathrm{cm}}$ in Figure 6 suggest that the maximum value of α occured between phase 0.5–0.6, just in the middle of the flux density rise. On the other hand, in spite of the scarcity of the data at 90 cm, the $\alpha_{90-20\mathrm{cm}}$ plot has a variability trend similar to that of $\alpha_{20-6\mathrm{cm}}$ and is the only spectral index observed to be positive even during the decay of the main outburst. This suggests that the turnover frequency of the LSI +61°303 synchrotron spectrum is likely to occur between 0.3 and 1.4 GHz throughout all the radio period.

At intermediate frequencies, $\alpha_{6-3.5\mathrm{cm}}$ remains quite constant and negative at the -0.5 value, indicating that LSI +61°303 is always optically thin between 6 and 3.5 cm, even during the onset of the radio outburst. As suggested by Taylor & Gregory (1984) and modelled by Paredes et al. (1991), this behavior is consistent with continuous injection of relativistic electrons in order to account for the flux density rise at optically thin frequencies.

At the highest frequencies, both $\alpha_{3.5-2\mathrm{cm}}$ and $\alpha_{2-1.3\mathrm{cm}}$ are always negative but not constant. The spectral index changes at these optically thin frequencies are likely to be related to the energy evolution of the relativistic electrons undergoing energy losses of different type. The energy loss mechanisms that have the strongest effect on the high frequency steepening of the radio spectrum are synchrotron radiation and inverse Compton losses (Pacholczyk, 1970), due to their energy square dependence. Since an electron with energy E radiates mainly at a characteristic frequency $\nu_c \propto E^2$, the effect of energy losses will be noticeable first at higher frequencies, where the radiating electrons will lose their energy more rapidly. In this way, once the injection process is over and energetic electrons are no longer replaced, one expects a progressive high frequency steepening of the spectrum during the decay of the outburst (Paredes, Peracaula & Martí 1997).

This expectation is actually confirmed by observations, especially by the $\alpha_{2-1.3\mathrm{cm}}$ plot of Figure 6, where the deep minima at phases 0.1 and 0.7 correspond to significant steepening of the spectrum during the decay of both the first minor and main outburst. There is also evidence of steepening during the decay of the second and third minor outbursts, at phases 0.35 and 0.95, but this is not so pronounced. In addition, the $\alpha_{3.5-2.0\mathrm{cm}}$ plot has also indications of similar steepening, but the dips of this curve are not so clear and they seem to occur slightly later in time than those of $\alpha_{2-1.3\mathrm{cm}}$, as expected as we go towards lower frequencies.

It is also important to remark that, following each $\alpha_{2-1.3\mathrm{cm}}$ steepening, the recovery of this spectral index leaves the 1.3 cm flux density at a value higher than expected from a simple extrapolation using the nearby $\alpha_{3.5-2.0\mathrm{cm}}$. This can be seen several times in the Figure 5 plots, at phases 0.97, 0.19, 0.42 and 0.79. We note that all these phases correspond to the onset of a flaring event or to its very early rise in the case of the main outburst. So, we speculate that these 1.3 cm flux density "excesses" could be attributed to the first stages of the particle injection process, when very fresh and short-lived highly energetic electrons are being produced and injected into the plasmon.

Overall, particle-injection from super-Eddington accretion can apparently explain the shape of the radio light curve observed in the system. However, the paucity of X-ray emission from LSI +61°303 both in the soft (Taylor et al. 1996) and hard bands (Tavani et al. 1996) does not agree with the expected flux from a compact object accreting at super-Eddington rates. Recently discovered superluminal jet X-ray transients GRS 1915+105 (Mirabel & Rodriguez 1994) and GRO J1655-40 (Hjellming & Rupen 1995) are characterized by strong hard X-ray outbursts in coincidence with relativistic plasmoid ejections. BATSE continuous monitoring of 2CG 135+1 in the hard X-ray range has established an upper limit of $\sim$ 10mCrab (20-100 keV) during the period April 1991-January 1995 (Tavani et al. 1996). This BATSE upper limit is more than two orders of magnitude lower than the expected flux from a super-Eddington accreting source similar to the Galactic superluminal X-ray transients (at the distance of LSI +61°303). Furthermore, the observed small column density of LSI +61°303, $N_H \sim 6 \cdot 10^{21}\,\mathrm{cm}^{-2}$ as deduced from ROSAT (Goldoni & Mereghetti 1995, Taylor et al., 1996) and ASCA observations (Leahy et al. 1996), is consistent with negligible intrinsic absorption at the source. No Fe X-ray line emission was detected by ASCA in coincidence with a radio flare (Leahy et al. 1996). We therefore conclude that if 2CG 135+1 is related to an accreting source, its properties must be quite different from those of GRS 1915+105 and GRO J1655-40 or other currently known accreting X-ray sources.

3.3. Optical and Infrared emission

Paredes et al. (1994) proposed that various features in the optical spectra of LSI +61°303 and its infrared flux were modulated with the radio period of the system. Our optical and infrared observations allow us to begin to test those claims and search for evidence of mass ejections from the system correlated with the radio outbursts, as would be predicted by the super-Eddington model.

3.3.1. Hα measurements

Figure 7 shows the Hα line profiles obtained during the observations. The profile is double peaked, with the red peak appreciably stronger than the blue in both spectra. In addition, broad wings to the Hα line are apparent in both spectra. A general discussion of the appearance of the spectrum of this source, with particular emphasis on the Hα line, is given by Gregory et al. (1979) and Paredes et al. (1994). Comparison of our spectra with those presented by Paredes et al. (1994), which cover all radio phases, shows the basic appearance unchanged since 1989. A more quantitive comparison of the new spectra, both with each other and with the historical spectra, may be made by fitting appropriate functions to the profile. However, in carrying out this comparison it is important to remember that many isolated (i.e. non-binary) Be stars show variations very similar to those described here, and that any attempt to correlate these with the orbital phase using the small sample of data presented here will necessarily be unreliable. This is, however, the first optical data obtained simultaneously with high energy observations, and is, as such, of interest.

The Hα fit was carried out using the DIPSO emission line fitting (ELF) routines described by Howarth & Murray (1991). We found that the Hα line is well represented by a combination of red and blue narrow (FWHM$\sim$ 5 Å) and single broad (FWHM$\sim$ 20Å) Gaussian components. Based on similar fits to their data, Paredes et al. (1994) discuss the possible origin of the three components in a disk surrounding the Be star, with the two narrow components arising naturally from rotation of the disk and the broad component due to electron scattered photons. The derived fit parameters are listed in Table 6, and the fits themselves overplotted on the spectra of Figure 7. Note that no attempt was made when calibrating the spectra to account for 'slit' and other losses. The absolute calibration of the flux values from night to night will therefore vary considerably. To allow for this we list the interpolated continuum flux value at the centre of the Hα line for each spectrum. Using these values allows the conversion of the measured fluxes into equivalent widths (which are independent of the flux calibration).

From the table no significant changes are found in the central wavelengths of the three Gaussians between the observations. However the FWHM of the red component increases from 4.5 to 5.8 Å between radio phases 0.56 and 0.64. Similar behavior was seen by Paredes et al. (1994), who observed an increase in FWHM$_r$ from 6 to 8 Å between phases 0.5 to 0.7. They suggested that this broadening of the red peak near radio maximum may be caused by an unresolved component of gas ejected from the system at that time. We note however that no significant change in the separation of the red and blue peaks (expressed on the figure in terms of the velocity v_r-v_b) is seen in our data, which might be expected if this were the case.

The V/R ratio is a standard quantity used in the analysis of Be star spectra, and is defined as the ratio of the peak fluxes of the blue and red components. In this case we use the peaks of the fitted components, and find the ratio increases from 0.6 ± 0.1 to 0.8 ± 0.1 between radio phases 0.56 to 0.64. This result is consistent with a constant V/R value.

The total Hα equivalent width derived from the fit parameters is also shown on Figure 7. A slight decrease in the Hα EW by $\sim$ 1 Å between the two spectra is apparent. This is again consistent with the pattern for similar radio phases reported by Paredes et al. (1994), and will be further discussed below in conjunction with the Hβ and Hγ observations of the source.

3.3.2. Hβ and Hγ measurements

In Figure 8 we plot our observations of the Hβ and Hγ lines from the source. Hβ shows a typical Be 'shell' spectrum with a deep central absorption core and two prominent wings. In both Hβ spectra the red wing is considerably stronger than the blue. We also note possible evidence for a weak, very broad blue wing, presumably analogous to the broad component in the Hα spectrum, which is also slightly blue shifted according to its derived central wavelength. The Hγ line is in absorption, although it is likely that some 'in-filling' of the line due to emission is present.

Due to the poorer signal-to-noise ratio of these spectra, it is not feasible to fit Gaussian profiles to either the Hβ or Hγ lines. Instead we measure total line equivalent widths using the FIGARO routine ABLINE (Robertson 1986). The resulting EWs are given on the plots of the spectra. A similar change is apparent in the EWs of both the Hβ and Hγ lines between the two nights, namely a decrease in the (emission) equivalent width of both lines by $\sim$ 0.5 Å. This occurs between radio phases 0.60 and 0.67. In the previous section we noted that the Hα EW decreased by $\sim$ 1 Å between phases 0.56 and 0.64. It therefore appears that the emission strengths of all of the Balmer recombination lines decreased steadily from radio phase 0.56 to 0.67. Whether this behavior is in fact a function of orbital phase, or merely represents uncorrelated variations in the circumstellar conditions, is naturally uncertain with the present dataset. However, it is encouraging that changes can be reliably measured on such a short time scale, and shows that a spectroscopic study of the system throughout a complete radio cycle would be extremely valuable. Such a study would also allow a redetermination of the orbital parameters of the system, which are currently based on the determination of Hutchings & Crampton (1981).

3.3.3. Infrared photometry

As shown in Figure 9, the source brightens in IR between radio phases 0.44 and 0.67. This may be due to either some form of re-processing of the radio flux during the outburst (a negative search for similar behavior in the source EXO2030+375 is reported by Norton et al. 1994), or some type of eclipse within the system. Examination of the folded infrared light-curve presented by Paredes et al. (1994) shows that the infrared variability of the source is more likely to be the result of some form of eclipse in the system, with the eclipse occurring between radio phases $\sim$ 0.3 and $\sim$ 0.5. The new data presented here do not allow us to either confirm or deny the eclipse interpretation. A complete set of observations through a single phase cycle will be necessary to properly understand the infrared variability of the system. In particular, it is important to note that superimposed on any possible orbital modulation will be long term variations in the infrared flux from the system. Therefore any inferences drawn from the folded light curve of Paredes et al. (1994) must be treated with some caution.

3.3.4. Optical line emission and high energy flux

One possible mechanism to account for the Hα variability we observe is reprocessing of the X-ray flux from the system. Apparao (1991) has shown that the presence of an X-ray emitting source embedded in a Be star wind should create an H II region in the wind which would emit optical line and continuum radiation. Using our total Hα flux density of $\sim$ 3700mJy, the radio derived distance to the system (2.0 kpc - Frail & Hjellming 1991) and an extinction derived from the color excess ($E(B-V) \sim 1.13$ Paredes & Figueras 1986) we derive a total Hα emission from the system of $\sim 10^{35}$ ergs/s. The ASCA 2 to 10 keV flux is however substantially less at 5×10^{33} ergs/s (Leahy et al. 1996). Therefore a maximum Hα variability of only 5 per-cent of the line EW is likely to be attributable to reprocessing of high energy flux. In addition, we note the efficiency for the processing of X-ray to Hα flux presented by Apparao (1991), which (although obviously dependant on the physical conditions and the input X-ray spectrum) is generally $\sim$ 0.05. A more reasonable estimate of the expected effect of reprocessing in this system may therefore be $\sim$ 0.2 percent of the EW.

We observe a total decline in Hα EW of around 10 per-cent over 2 days in the system and the evidence from the Hβ and γ lines is that the Balmer series emission declined further the following day. We therefore estimate a total decline of 15 per-cent in the Hα EW over three days, substantially higher than our derived maximum of 5 percent from the previous paragraph. We therefore conclude that the Hα variability we observe from the system is unlikely to be due to reprocessing of the variable X-ray flux, and the most likely explanation is that it is simply the normal variability associated with the Be phenomenon. An analogous calculation made for the IR flux from the system yields the same result.

4. Conclusions

This paper has discussed the results of a multiwavelength monitoring campaign on the radio/X-ray/Be binary LSI +61°303 and the γ-ray source 2CG 135+1. The original aim of the campaign was to prove the association between the two sources, either by spectral or temporal signatures. We observed the source three times using the OSSE detector on CGRO, but only detected it during the first observation. The OSSE data for the field containing

2CG 135+1 have insufficient signal-to-noise ratio to search for any correlation with the radio light curve of LSI +61°303. A comparison of the OSSE spectrum from the direction of 2CG 135+1 with spectra of LSI +61°303 at lower and higher energies (as determined by ROSAT, ASCA and EGRET) does not allow an unambiguous association between these two sources. We notice that a substantial part of the high-energy flux detected by OSSE and COMPTEL might originate from QSO 0241+622. Future observations of the 2CG 135+1 field with OSSE (using different collimator orientations) and with the ROSSI X-ray Timing Explorer and SAX (which have a smaller fields of view) may help resolve this issue.

We also discussed the implications of our radio, optical and infrared observations of LSI +61°303. We have shown that the models proposed to explain the features of the LSI +61°303 system (super-Eddington neutron star accretion and a non-accreting shock-driven young pulsar system) are able to qualitatively explain the features of the observed multifrequency radio lightcurves. More data are required to resolve the outstanding issues concerning this system. We also notice that the study of the radio spectrum of LSI +61°303 deserves more attention in order to better understand the physics of the acceleration of radio emitting electrons. In particular, it would be very interesting to carry out multi-frequency monitoring of a full outburst including simultaneously both the the centimeter and millimeter wavelength domain. The optical spectroscopy and infrared photometry have shown that genuine night-to-night variability is also present. An orbit-long monitoring campaign at these wavelengths would be very useful in determining whether the observed variability was truly correlated with orbital phase.

5. Acknowledgements

Research partially supported by the GRO Guest Investigator Program (grant NAG-5-2729). JMP acknowledges support by DGICYT (PB94-0904). JM is supported by a postdoctoral fellowship of the Spanish Ministerio de Educación y Cultura. The NRAO is operated by Associated Universities, Inc., under cooperative agreement with the National Science Foundation. The JKT is operated by the Royal Observatory, Greenwich on behalf of the UK PPARC. The TCS is operated by the Instituto de Astrofísica de Canarias, Tenerife. Some of the data reduction for this paper was carried out using the Southampton University STARLINK node.

REFERENCES

Apparao, K.M.V 1991, ApJ, 376, 256

Bignami, G.F., et al. 1981, ApJ, 247, L85

Edwin, R. 1988, RBS User Manual, La Palma User Manual 11, Royal Greenwich Observatory

Frail, D.A. & Hjellming, R.M. 1991, AJ, 101, 2126

Goldoni, P. & Mereghetti, S. 1995, A&A, in press

Gregory, P.C., et al. 1979, AJ, 84, 1030

Harrison, F.A., Leahy, D.A. & Waltman, E.B. 1996, ApJ, submitted

Hermsen, W., et al. 1977, Nat., 269, 494

Howarth, I.D. & Murray J. 1991, Starlink User Note 50.13, DIPSO - A friendly spectrum analysis program, Rutherford Appleton Laboratory

Hutchings, J.B. & Crampton D. 1981, PASP, 93, 486

Johnson, W.N., et al. 1993, ApJ Suppl., 86, 693

Kniffen, D., et al. 1997, ApJ Letters, in press

Leahy, D.A., Harrrison, F.A. & Yoshida, A. 1996, ApJ, submitted

Lipunov, V.M. & Nazin, S.N. 1994, A&A, 289, 822

Maraschi, L., Treves, A. 1981, MNRAS, 194, 1P

Martí, J. & Paredes, J.M. 1995, A&A 298, 151

Negueruela, I., et al. 1997, MNRAS, 284, 859

Nolan, P.L., et al. 1993, ApJ, 409, 697

Norton, A.J., et al. 1994, MNRAS, 271, 981

Oke, J.B. & Gunn, J.E. 1983, ApJ, 266, 713

Pacholczyk, A.G. 1970, *Radio Astrophysics*, Freeman and Company, San Francisco

Paredes, J.M. & Figueras, F. 1986, A&A, 154, L30

Paredes, J.M., Martí, J., Estalella, R., Sarrate J. 1991, A&A 248, 124

Paredes, J.M., et al. 1994 A&A, 288, 519

Paredes, J.M., Martí, J., Peracaula, M., Ribó, M. 1997, A&A, 320, L25

Paredes, J.M., Peracaula, M. & Martí, J. 1997, Proc. 2nd INTEGRAL Workshop, ESA SP-382, 319

Penninx, W. 1989, *Proceedings of the 23rd ESLAB Symposium on two topics on X-Ray Astronomy*, Vol. 1, ESA SP-296, p. 194

Perotti, F. et al. 1980, ApJ, 239, L49

Ray, P.S., Foster, R.S., Waltman, E.B., Ghigo, F.D., Tavani, M. 1997, ApJ, submitted

Robertson, J.G. 1986, PASP, 98, 1220

Share, G.H., et al. 1979, in proc. 21st COSPAR meetings, (Innsbruck), eds. W.A. Bally, L.E. Peterson, (New York: Academic), p. 535

Shortridge, K. 1991, STARLINK MUD, Figaro - General Data Reduction Analysis, Rutherford Appleton Laboratory

Swanenburg, B.N., et al. 1981, ApJ, 243, L69

Tavani, M. 1995, in "The Gamma-Ray Sky with COMPTON GRO and SIGMA", eds. M. Signore, P. Salati, G. Vedrenne, (Dordrecht: Kluwer Academic), p. 181

Tavani, M., et al. 1996, A&A, 120, 243

Tavani, M. 1997, in "The many faces of neutron stars", ed. R. Buccheri (Dordrecht: Kluwer Academic), in press

Tavani, M. & Arons J. 1997, ApJ, 477, 439

Taylor, A.R. & Gregory P.C. 1982, ApJ, 255, 210

Taylor, A.R. & Gregory P.C. 1984, ApJ, 283, 273

Taylor, A.R., Kenny H.T., Spencer R.E., Tzioumis, A. 1992, ApJ, 395, 268

Taylor, A.R., Young G., Peracaula M., Kenny H.T., Gregory P.C. 1996, A&A, 305, 817

Thompson, D., et al. 1995, ApJS, 101, 259

Turner, M.J. & Pounds, K.A. 1989, MNRAS, 240, 833

van Dijk, R., et al. 1996, A&A, 315, 485

von Montigny, C., et al. 1993 IAU Circ 5708

This 2-column preprint was prepared with the AAS LaTeX macros v4.0.

Table 1: OSSE Observations of 2CG 135+1

VP	Dates	Radio Phase	Exposure
325	April 26 – May 10 1994	0.31 – 0.84	3.30×10^5 s
330	June 10 – June 14 1994	0.01 – 0.16	0.98×10^5 s
332	June 18 – July 5 1994	0.32 – 0.95	3.60×10^5 s

Table 2: OSSE Flux measurements and upper limits

	Flux (photons-cm^{-2}-s^{-1}-MeV^{-1})				
VP	0.05–0.1 MeV	0.1–0.17 MeV	0.17–0.3 MeV	0.3–1.5 MeV	1.5–10 MeV
325	$4 \pm 2 \times 10^{-3}$	$1.2 \pm 0.5 \times 10^{-3}$	$1.0 \pm 0.5 \times 10^{-3}$	$1.4 \pm 1.5 \times 10^{-4}$	$0.5 \pm 1.6 \times 10^{-5}$
330	$2 \pm 3 \times 10^{-3}$	$-0.2 \pm 0.9 \times 10^{-3}$	$0.2 \pm 0.7 \times 10^{-3}$	$1 \pm 2 \times 10^{-4}$	$-0.3 \pm 2.5 \times 10^{-5}$
332	$3 \pm 2 \times 10^{-3}$	$0.6 \pm 0.5 \times 10^{-3}$	$-0.5 \pm 0.4 \times 10^{-3}$	$0.8 \pm 1.3 \times 10^{-4}$	$1 \pm 1 \times 10^{-5}$

Table 3: Multifrequency VLA Radio Observations of LSI +61°303

MJD	Radio Phase	S_{90cm} (mJy)	S_{20cm} (mJy)	S_{6cm} (mJy)	$S_{3.5cm}$ (mJy)	$S_{2.0cm}$ (mJy)	$S_{1.3cm}$ (mJy)
49512.93	0.97		54.4 ± 0.4	30.5 ± 0.1	21.71 ± 0.05	14.8 ± 0.2	13.5 ± 0.5
49515.34	0.06		69.8 ± 0.5	43.1 ± 0.1	32.87 ± 0.07	17.6 ± 0.4	8.3 ± 0.5
49516.34	0.09		48.7 ± 0.4	30.8 ± 0.1	22.76 ± 0.05	12.7 ± 0.2	5.0 ± 0.4
49518.96	0.19		35.9 ± 0.4	27.4 ± 0.1	21.15 ± 0.05	16.0 ± 0.2	14.8 ± 0.4
49521.34	0.28		57.7 ± 0.5	33.3 ± 0.1	25.43 ± 0.05		
49522.17	0.31		65.3 ± 0.4	44.6 ± 0.1	36.00 ± 0.05		
49523.16	0.35		43.2 ± 0.4	42.0 ± 0.1	33.16 ± 0.06	26.2 ± 0.2	20.6 ± 0.5
49525.05	0.42		75.4 ± 0.4	63.1 ± 0.1	48.56 ± 0.08	30.5 ± 0.2	25.3 ± 0.7
49530.28	0.62		146.6 ± 0.5	168.5 ± 0.1	134.50 ± 0.07	94.7 ± 0.2	71.4 ± 0.4
49532.28	0.70		158.6 ± 0.5	136.7 ± 0.1	104.13 ± 0.05	80.3 ± 0.3	35.7 ± 0.6
49534.87	0.79	106 ± 21	172.4 ± 0.5	107.9 ± 0.1	79.19 ± 0.06	55.1 ± 0.2	47.6 ± 0.5
49536.06	0.84		136.2 ± 0.4	97.5 ± 0.1	72.43 ± 0.05	52.4 ± 0.2	39.6 ± 0.4
49537.12	0.88	106 ± 23	137.3 ± 0.4	92.2 ± 0.1	68.70 ± 0.05	52.5 ± 0.2	40.0 ± 0.4
49539.13	0.95		115.7 ± 0.4	69.2 ± 0.1	51.03 ± 0.05	38.2 ± 0.2	26.9 ± 0.5
49540.96	0.02	61 ± 20	73.7 ± 0.5	41.8 ± 0.1	30.81 ± 0.05	21.6 ± 0.2	16.6 ± 0.4
49542.11	0.07		58.8 ± 0.4	36.4 ± 0.1	26.89 ± 0.05	19.6 ± 0.2	15.4 ± 0.4

Table 4: Log of Optical Spectroscopy

MJD	Radio Phase	λ (Å)	T_{exp} (s)
49528.7	0.56	6030 – 7070	1200
49529.7	0.60	4200 – 5200	1800
49530.7	0.64	6070 – 7040	1500
49531.7	0.67	4200 – 5200	1800

Table 5: Infrared Photometry

MJD	Radio Phase	J	H	K
49525.5	0.44	8.68± 0.02	8.28± 0.02	7.97± 0.02
49526.5	0.48	8.62± 0.02	8.21± 0.02	7.93± 0.02
49527.5	0.52	8.58± 0.03	8.19± 0.02	7.89± 0.03
49530.5	0.63	8.60± 0.05	8.19± 0.04	7.86± 0.03
49531.5	0.67	8.62± 0.04	8.22± 0.02	7.89± 0.02
49535.5	0.82	8.63± 0.12	8.23± 0.12	7.94± 0.08

Table 6: Hα fit parameters

MJD	49528.7	49530.7
λ_b (Å)	6657.53 ± 0.07	6657.56 ± 0.09
λ_r (Å)	6565.94 ± 0.04	6565.93 ± 0.09
λ_c (Å)	6560.88 ± 0.40	6561.12 ± 0.49
FWHM$_b$ (Å)	4.5 ± 0.2	3.5 ± 0.2
FWHM$_r$ (Å)	4.5 ± 0.2	5.8 ± 0.3
FWHM$_c$ (Å)	20.6 ± 1.1	26.7 ± 1.4
Peak$_b$ (mJy)	98 ± 5	135 ± 8
Peak$_r$ (mJy)	165 ± 5	172 ± 7
Peak$_c$ (mJy)	47±5	78 ± 7
Flux$_b$ (mJy)	474 ± 42	502 ± 49
Flux$_r$ (mJy)	794 ± 41	1060 ± 80
Flux$_c$ (mJy)	1050 ± 85	2180 ± 118
Continuum (mJy)	250 ± 10	450 ± 10

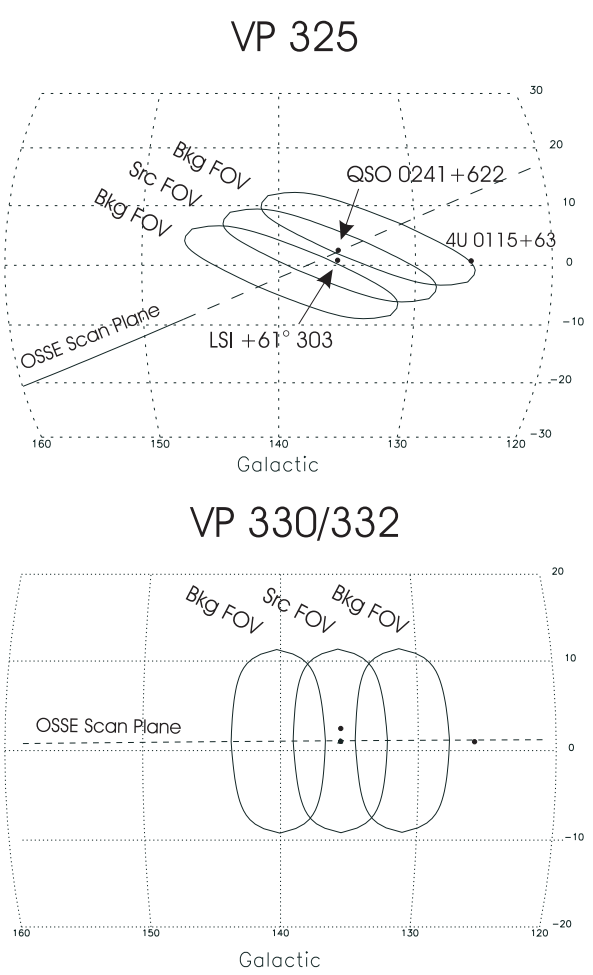

Fig. 1.— OSSE viewing configuration for VP 325, 330 and 332. The ovals represent 10% response contours for an OSSE detector. In each case, the source-pointing and two background-pointing fields are indicated.

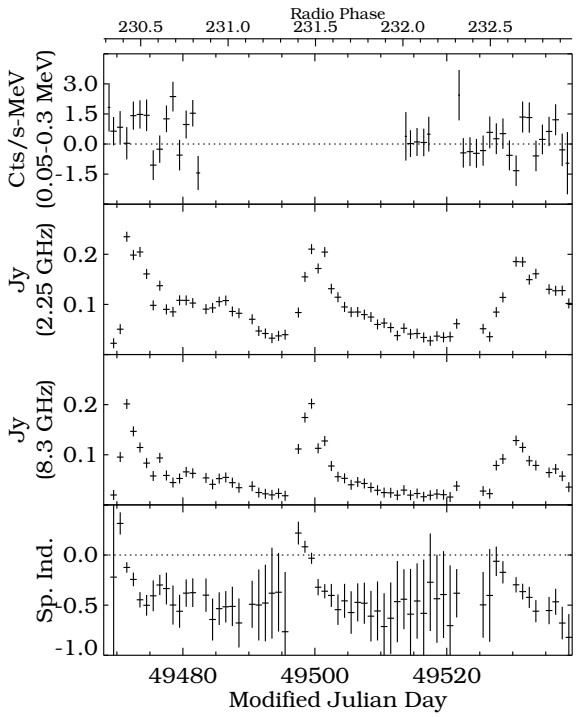

Fig. 2.— OSSE and GBI lightcurves. The lefthand group of OSSE points are VP 325, the first group on the right is VP 330 and the second group on the right is VP 332. The abscissa is labeled both with Modified Julian Day and with phase of the 26.496-day radio period (Taylor & Gregory 1984). The integer part of the phase is the number of cycles since the radio ephemeris epoch.

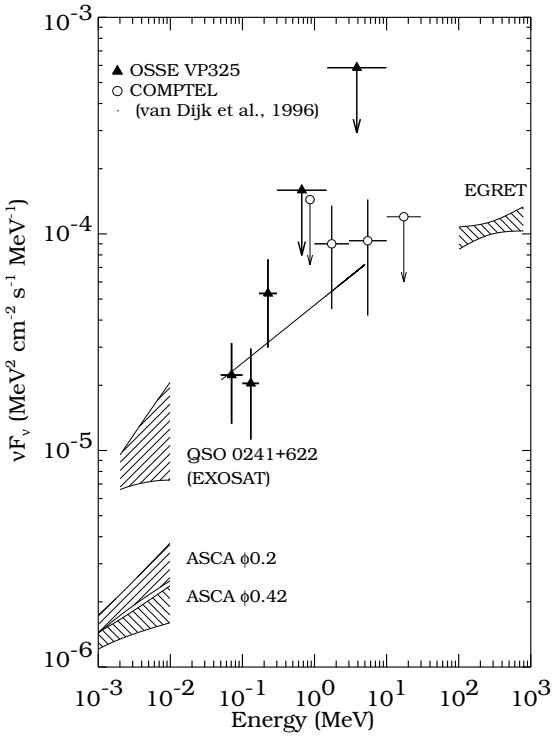

Fig. 3.— X-ray and γ-ray spectra from the region around LSI +61°303. Included are data from OSSE VP 325 (triangles together with best-fit power law) and COMPTEL (open circles). Also shown are results on LSI +61°303 from EGRET and ASCA. The lines labeled "EGRET" represent a best fit power law 68% confidence interval from Thompson et al. (1995), while the two sets of lines labeled "ASCA ϕ0.2" and "ASCA ϕ0.42" are 90% confidence intervals for ASCA measurements at radio binary phases 0.2 and 0.42 respectively (Leahy et al. 1996). The lines labeled "QSO 0241+622" are a 90% confidence interval of the EXOSAT spectrum from QSO 0241+622 (Turner & Pounds 1989).

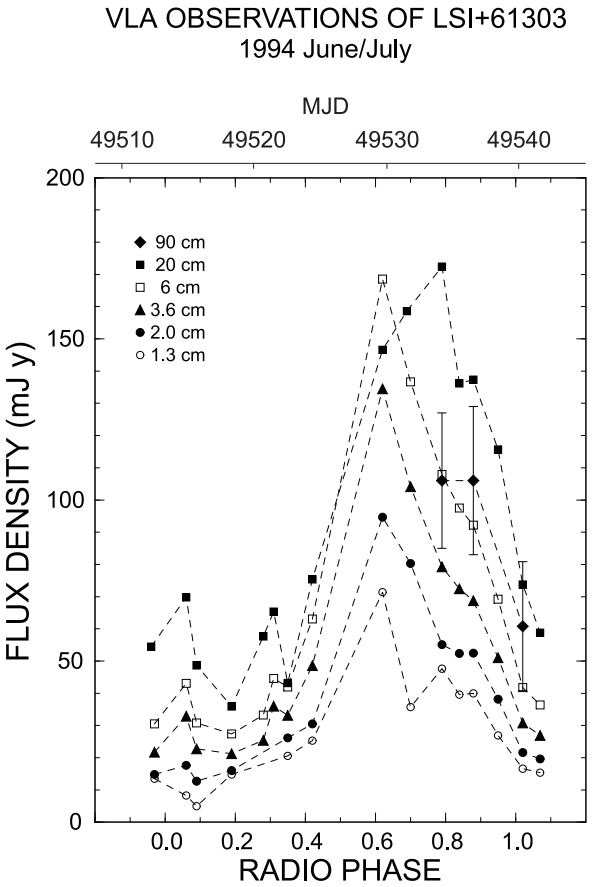

Fig. 4.— Multifrequency radio light curves of LSI +61°303 observed with the VLA corresponding to the radio outburst of 1994 June-July. Error bars not shown are smaller than the symbol size.

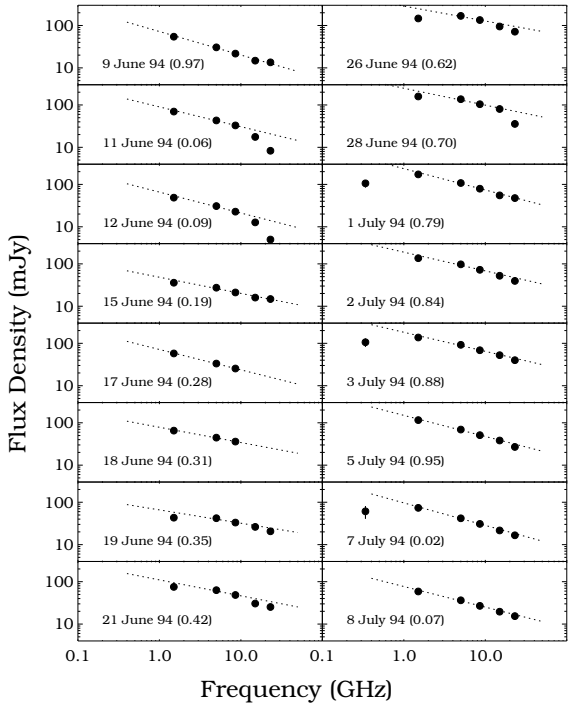

Fig. 5.— Time evolution of the LSI +61°303 non-thermal radio spectrum during the outburst of 1994 June-July. Spectra are labeled according to the date and radio phase of the observation.

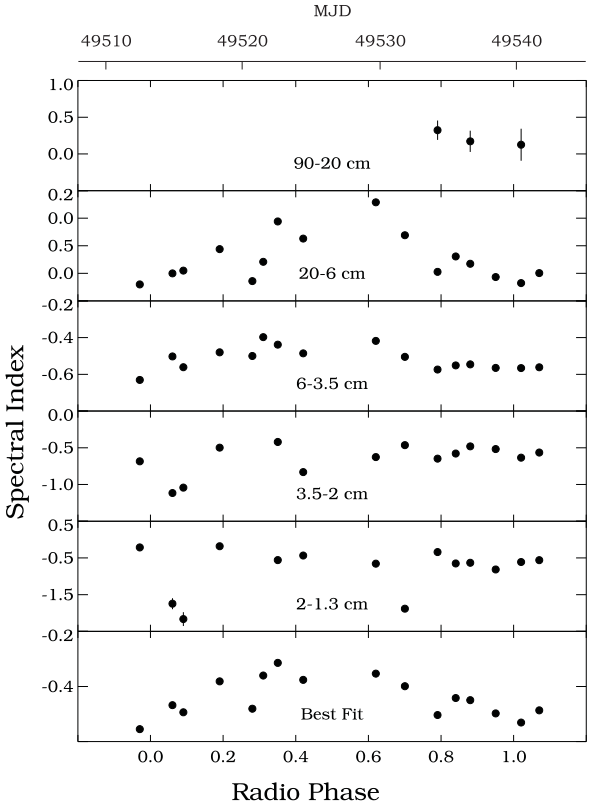

Fig. 6.— Time evolution of the spectral indices of LSI +61°303 during the outburst of 1994 June-July. They have been computed between all adjacent wavelength pairs.

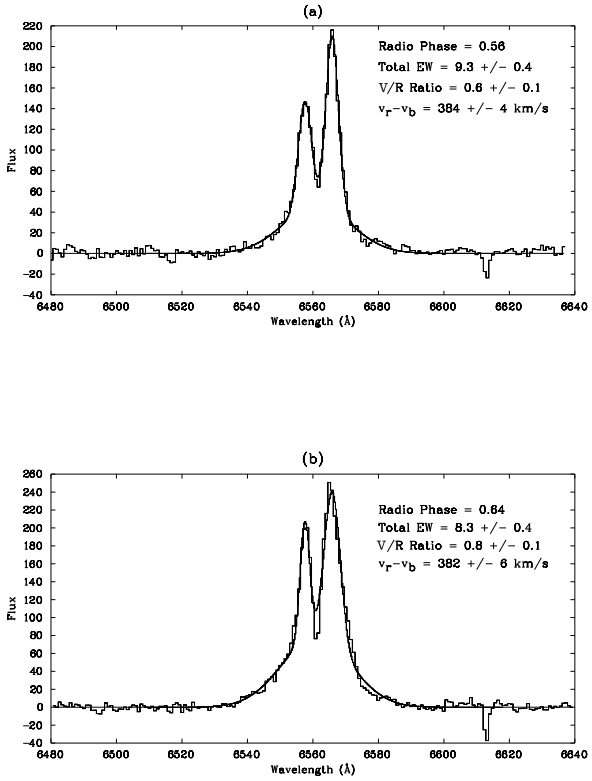

Fig. 7.— Details of the Hα profiles taken at two different binary phases. The vertical scales are in arbitrary flux units.

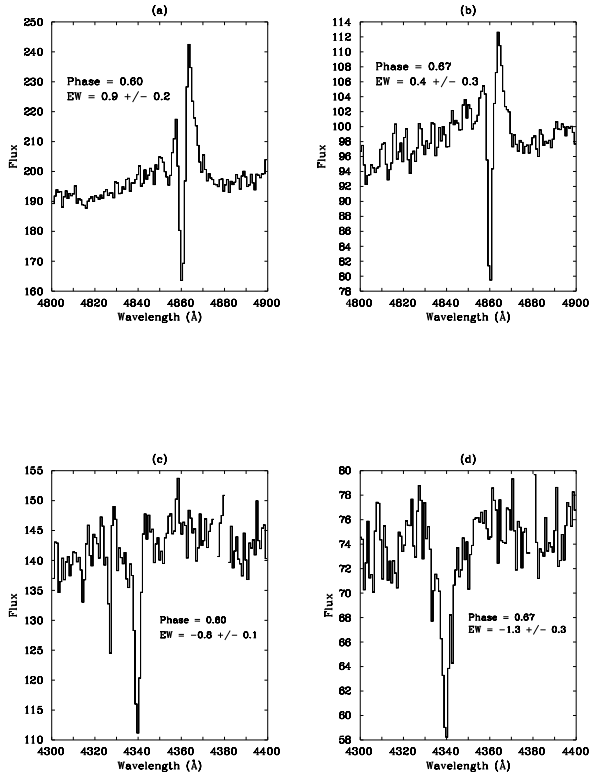

Fig. 8.— Details of the Hβ (panels (a) and (b)) & Hγ (panels (c) and (d)) profiles taken at two different binary phases. The vertical scales are in arbitrary flux units.

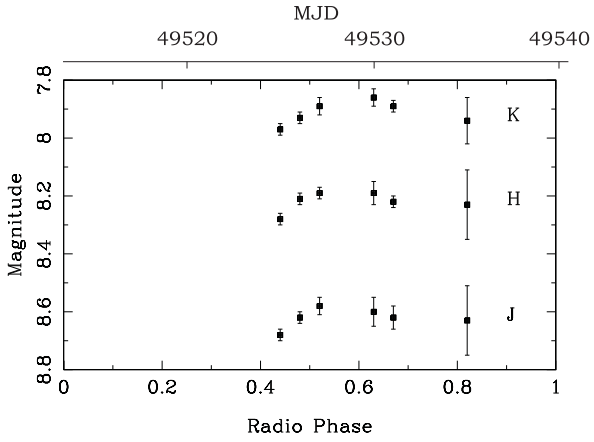

Fig. 9.— Infrared light curves of LSI +61°303